SEISMIC EVALUATION OF GROUTED SPLICE SLEEVE CONNECTION ALTERNATIVES FOR REINFORCED PRECAST CONCRETE BRIDGE PIERS IN ACCELERATED BRIDGE CONSTRUCTION

M. J. Ameli, Dept. of Civil and Environmental Eng., University of Utah
Joel E. Parks, Dept. of Civil and Environmental Eng., University of Utah
Dylan N. Brown, Michael Baker International, Madison, WI
Chris P. Pantelides, PhD, SE, Dept. of Civil and Environmental Eng., University of Utah

ABSTRACT

Precast concrete substructure elements such as columns and cap beams are frequently used in accelerated bridge construction. The connections between these precast elements must be able to withstand significant stresses and deformations in large earthquakes. Grouted splice sleeve connectors were used in various configurations to connect half-scale precast columns to footings, and precast columns to cap beams. A cyclic quasi-static load was applied to four column–to–footing and three column–to–cap beam connections. The column–to–footing connections incorporated a connector type with the bars grouted at both ends, while another type of connector with one bar fastened to one end, and the other bar grouted in the opposite end, was used in the column–to–cap beam connections. Splice sleeve connectors were located in the column ends for each connection category in the first phase of the experiments. In the second phase, they were located in the footing and the cap beam, to investigate the effect of the connector location in the overall response of the specimens under seismic loading. A debonded reinforcing bar zone was considered for the third test alternative of the column–to–footing connection. Two monolithic cast-in-place concrete specimens with identical details to the precast assemblies served as the control for each category. Test results indicate that a superior hysteretic response was achieved when the connectors were placed inside the footing or cap beam, as opposed to the column end. Debonding of reinforcing bars resulted in a more ductile response compared to all other precast alternatives.

Keywords: Accelerated Bridge Construction, Precast Substructure, Grouted Splice Sleeve, Connections, Mechanical Coupler, Cyclic Load Test.

INTRODUCTION

Accelerated Bridge Construction (ABC) refers to a bridge construction type that incorporates innovative techniques, methodologies, and materials to reduce the construction time and traffic disruption. It provides a higher level of work-zone safety for workers and commuters, and improves environmental-friendly activities. Prefabrication of bridge structural components is an effective method in this process and is one of the ABC methods under the category of Prefabricated Bridge Elements and Systems (PBES) promoted by the Federal Highway Administration (FHWA).

Connections between PBES are critical in maintaining the integrity of the bridge in seismic regions. These connections not only have to conform to ABC standards in terms of the overall construction delivery time, but must also resist high levels of earthquake-induced deformations and stresses. In recent years, research studies have been conducted on emulative connections between the prefabricated components of bridge bents. These connection types include grouted duct connections, pocket and socket connections, innovative techniques and hybrid connections, and bar coupler connections using mechanical splices, as described in NCHRP Report 698.[1]

Among typical bar couplers, Grouted Splice Sleeve (GSS) connectors have found applications in precast concrete construction because of ease of constructability and adequate tolerance.[2] The GSS connectors are hollow steel cylinders made of ductile iron. Reinforcing bars from two reinforced precast concrete components that are to be connected to each other are grouted at both sleeve ends, or fastened to one threaded end and grouted at the opposite end in the other type, as shown in Fig. 1. Such connectors have been used in bridge construction in non-seismic regions because they accelerate the construction process. Experimental studies have been conducted on various types of mechanical couplers comprising only two connecting bars, cast iron sleeve, and high-strength grout.[3-5]

Fig.1 Grouted Splice Sleeve (GSS) connectors

Such experiments, referred to as air tests, were conducted to study the strength, reinforcing bar slip, bond characteristics, and fatigue life of the mechanical couplers. Jansson (2008) reported a series of air tests on fastened and grouted splice sleeve connectors for No. 6 and No. 11 reinforcing bars. The tests showed acceptable performance in terms of reinforcing bar slip and fatigue life; all No. 6 assemblies failed due to fracture of the reinforcing bar in the threaded region, thereby reaching the nominal tensile strength of the bars.[3]

Cyclic tests were conducted on large-scale precast concrete specimens joined by means of various grouted splice sleeve connectors.[6-11] The presence of grouted splice sleeve connectors in the plastic hinge region did not considerably change the lateral force capacity of the assembly. However, the displacement capacity was found to be smaller than that of monolithic specimens. Damage progression and the plastic hinge mechanism were also different relative to monolithic specimens.

This paper presents experimental results of four quasi-static cyclic tests of half-scale column–to–footing specimens, three of which used grouted/grouted splice sleeve (GGSS) connectors, to investigate their performance compared with the fourth specimen, which was built using cast-in-place construction. In addition, experimental results of three quasi-static cyclic tests of half-scale column–to–cap beam specimens are presented, two of which used fastened/grouted splice sleeve (FGSS) connectors, and the third specimen was built using cast-in-place construction. The two types of GSS connectors are commercially available from two different manufacturers in the United States. Both connector types conform to ASTM A536 standards.

GSS connectors were incorporated in the column plastic hinge region of specimens GGSS-1 and FGSS-1. The GSS connectors were located in the footing and cap beam of specimens GGSS-2 and FGSS-2, respectively. GGSS-3 had a similar configuration to GGSS-1 but an intentional debonding was applied over 8 in. of the footing dowel bars (outside the connector). Control specimens GGSS-CIP and FGSS-CIP were constructed monolithically without any connectors or bar lap splices. Table 1 shows the test matrix and test configuration alternatives.

DETAILS OF SPECIMENS

The specimens were designed and detailed to simulate typical prototype bridges constructed in the State of Utah, following the AASHTO LRFD Bridge Design Specifications (2012), and the AASHTO Guide Specifications for LRFD Seismic Bridge Design (2011).[12, 13] A circular configuration of column longitudinal bars and an octagonal column cross section were adopted to facilitate the process of pre-casting the columns. Currently, the aforementioned design codes in addition to the Caltrans Seismic Design Criteria (SDC) inhibit the splicing of reinforcement, including mechanical anchorage devices, in the plastic

Table 1. Test Matrix

	Test ID	Connection Type	Designation	Connector Location	Other
Category I	1	Column-Footing	GGSS-1	In Column	
	2	Column-Footing	GGSS-2	In Footing	
	3	Column-Footing	GGSS-3	In Column	Unbonded reinforcing bars in footing
	4	Column-Footing	GGSS-CIP	NA	Cast-In-Place
Category II	5	Column-Cap Beam	FGSS-1	In Column	
	6	Column-Cap Beam	FGSS-2	In Cap beam	
	7	Column-Cap Beam	FGSS-CIP	NA	Cast-In-Place

hinge region of ductile members, for bridges located in moderate-to-high seismic areas.[14] In the AASHTO Guide Specifications for LRFD Seismic Bridge Design (2011), this would apply to Seismic Design Categories (SDCs) C and D. Thus, the preliminary design and detailing was developed for assemblies without any type of GSS, i.e. cast-in-place specimens for each category. The design was then adjusted to accommodate the GSS connectors within the precast specimens as needed, and essential modifications were considered accordingly.

The specimens were half-scale models of common prototype highway bridges, specifically the Riverdale Road Bridge over I-84 in Utah. The column, footing, and cap beam dimensions and main longitudinal bars and their configuration were acquired by considering 50% of the actual properties. The column height for all specimens was 8 ft 6 in. with a 21 in. octagonal cross section to facilitate casting. The top 18 in. of the column was changed to a 21 in. square for testing. Six No. 8 bars in a circular arrangement and a No. 4 spiral with a pitch of 2½ in. made up the column reinforcement. The longitudinal and volumetric transverse reinforcement ratios were 1.3% and 1.9%, respectively.

The footing was designed as a 6-ft long x 3-ft wide x 2-ft deep precast concrete element and consisted of No. 8 longitudinal bars enclosed by No. 4 double hoops. The cap beam was designed as a 9-ft long x 2-ft wide x 2-ft deep precast pier cap; it had the same reinforcing bar size and arrangement as the footing. The footing and cap beam were designed to remain linearly elastic and not undergo plastic deformations. The design inhibits shear failure from occurring in the column by using a shear span-to-depth ratio of more than 5.0 (corresponding

to slender columns) along with closely spaced adequate shear reinforcement. The desirable column failure mode was set to be either flexural or splice failure.

Fig. 2 shows specimen details for Category I (column–to–footing) in which GGSS connectors were incorporated at the interface of the three precast specimens. The specimen details in Category II (column–to–cap beam) are shown in Fig. 3. The FGSS connectors were used in two different configurations to connect the precast specimens.

The GSS connectors were embedded in the column plastic hinge region for specimens GGSS-1, GGSS-3, and FGSS-1, with dowel bars projecting 7 in. from the precast footing and cap beam. A postgrout operation was conducted for the aforementioned specimens using proprietary high-strength grout provided by the cast-iron sleeve manufacturers. In postgrout operations the grout is pumped into the bottom nozzle of the connectors and travels up against gravity to fill the inside space of the connector. The GSS connectors were located in the footing and cap beam of specimens GGSS-2 and FGSS-2, respectively. A pregrout technique was implemented for these two specimens to facilitate installation. Both inlet and outlet ports of the six connectors were sealed during construction of the footing and cap beam reinforcing bar cages of the two specimens. During erection of specimens GGSS-2 and FGSS-2 and before lowering and positioning the column, the high-strength grout was pumped into the wide end opening of the embedded connectors.

EXPERIMENTAL SETUP AND DISPLACEMENT HISTORY

The specimens were attached to the test frame using high strength bolts; the lateral cyclic load and axial load were simultaneously applied to the column top. A 120-kip servo-controlled actuator, with an overall stroke of 18 in. applied the cyclic load to the precast specimens; the control specimens were tested using a 250-kip servo-controlled actuator with an overall stroke of 24 in. All tests were carried out using displacement control. An axial load of 6% of the column compressive capacity was applied to simulate gravity loads. An actuator placed on top of the column, applied the compression force to a steel spreader beam which was connected to two high strength threaded rods, as shown in the test setup of Fig. 4.

For ease of construction and testing, all column–to–cap beam specimens (Category II) were assembled and tested in an inverted position. The displacement history was composed of increasing amplitudes of the predicted column yield displacement.[15] Two cycles were employed for each displacement step to the east and west. The displacement rate was set to 1.2 in./min up to the end of the 3% drift ratio, after which it was changed to 4 in./min. Fig. 5 shows the displacement history in terms of cycles and drift ratios.

Tension tests of reinforcing bars were conducted along with compression tests on concrete cylinders and grout cubes for each specimen.[16-18] The column longitudinal reinforcing bars

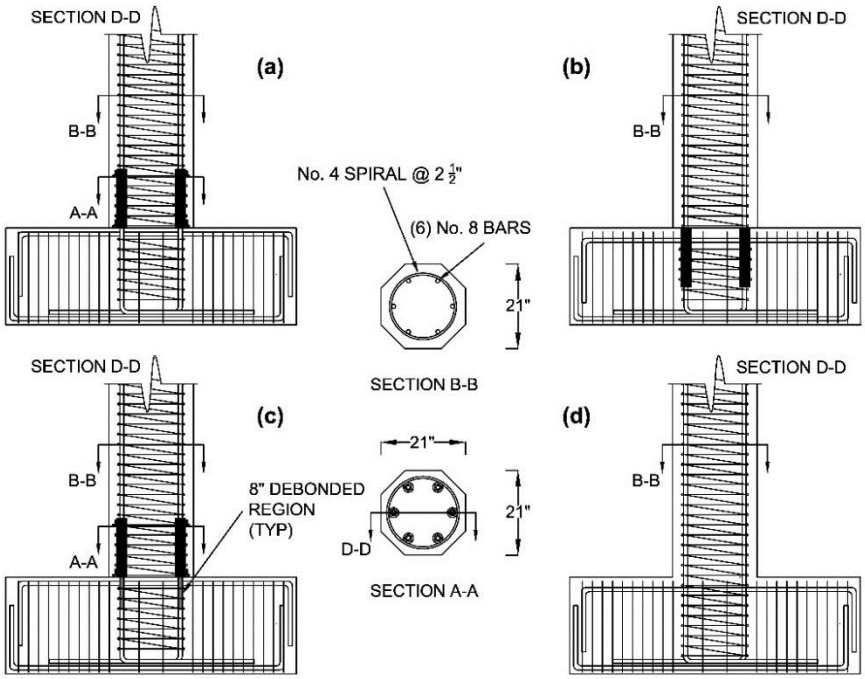

Fig. 2 Details for Category I (column–to–footing) specimens: (a) GGSS-1, (b) GGSS-2, (c) GGSS-3, and (d) GGSS-CIP

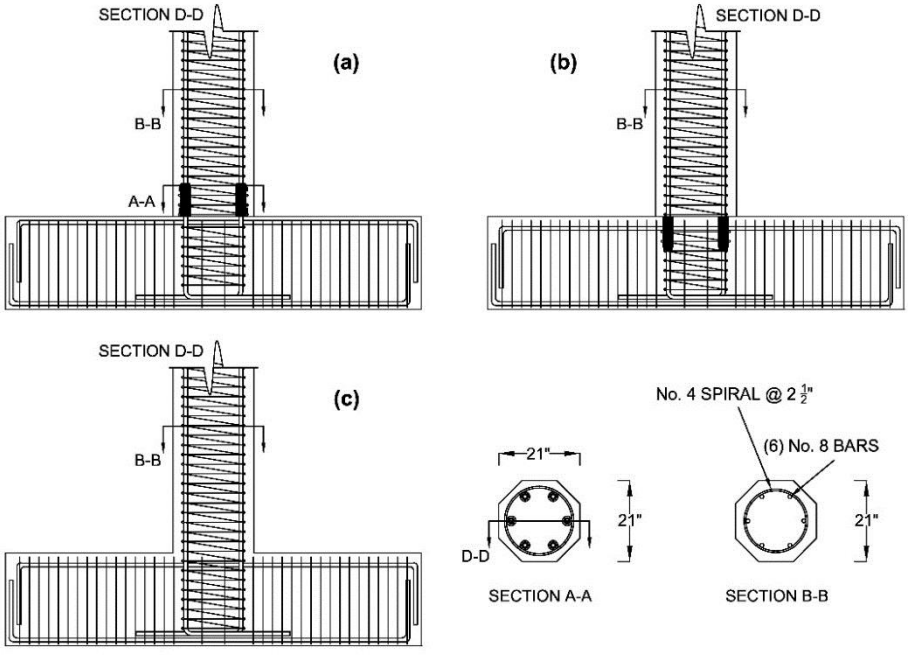

Fig. 3 Details for Category II (column–to–cap beam) specimens: (a) FGSS-1, (b) FGSS-2, and (c) FGSS-CIP

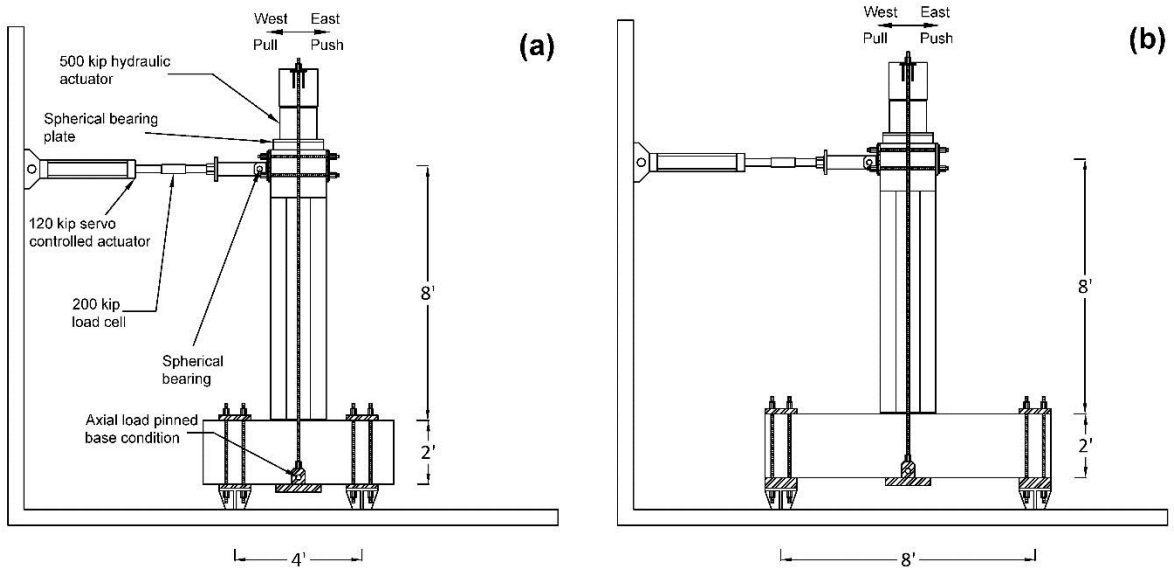

Fig. 4 Experimental setup: (a) Category I (column–to–footing), (b) Category II (column–to–cap beam)

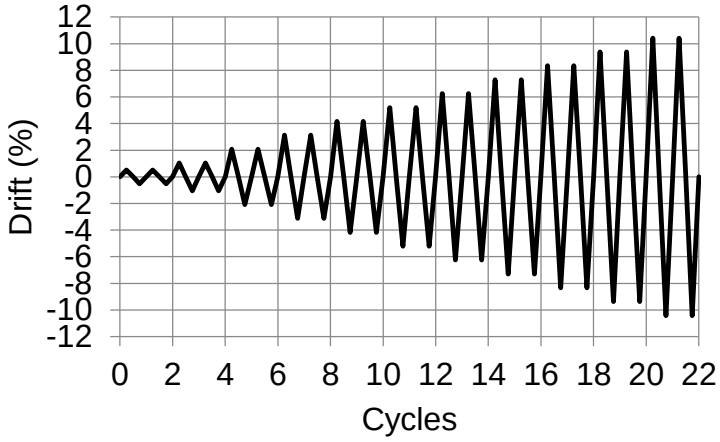

Fig. 5 Displacement history

of all specimens except FGSS-1 had a yield and ultimate strength of 68 ksi and 93 ksi, respectively. The column bars for specimen FGSS-1 were obtained from the manufacturer with a customized threaded end and had different yield and ultimate strengths equal to 77 ksi and 102 ksi, respectively. Table 2 contains the compression test results for the concrete and grout reported for both the 28th day of curing and test day of the specific test.

TEST RESULTS

EXPERIMENTAL OBSERVATIONS AND HYSTERETIC RESPONSE—CATEGORY I

Fig. 6 shows the hysteresis curves of the column–to–footing specimens. They include three major damage states: concrete cracking and spalling, yield penetration, and reinforcing bar fracture.

Response of GGSS-1

A minor hairline crack developed at the bed grout, located at the column–to–footing interface of GGSS-1, during the 0.5% drift ratio. This crack became wider and was accompanied by another crack forming right above the connectors during the first cycle of the 1% drift ratio. Spalling initiated during the first cycle of the 3% drift ratio and progressed near the corners of the octagonal column. Cracks widened and spalling progressed at higher drift ratios. The crack which had formed above the connectors had a width of 0.013 in. at a drift ratio of 4%, a width of 0.02 in. at a drift ratio of 5%, and 0.03 in. at the 6% drift ratio.

There were only a few flexural cracks at the column base as damage was localized over the column–to–footing interface and the section above the connectors. Yield penetration was noted at the end of the 6% drift ratio up to a depth of 1.5 in. and 1 in. on the west and east side of the column, respectively. The height of the spalled region was 8 in. and 14 in. on the west and east side of the column, respectively. The column spiral of GGSS-1 became visible during the 7% drift ratio. The bed grout deteriorated around the perimeter of the column end, while the spalled region over the connectors became deeper and the GGSS connectors were visible at the end of the 8% drift ratio; the two extreme footing dowels fractured shortly after the 8% drift ratio at a location 1.0 to 1.5 in. below the surface of the footing, where there was no confining transverse reinforcement. Fig. 7(a) shows the state of damage at failure.

Table 2. Compressive strength of concrete and grout (ksi)

	Specimen	**Concrete**		**Grout**	
		28-day	**Test day**	**28-day**	**Test day**
Category I	GGSS-1	5.3	5.9	14.4	14.4
	GGSS-2	3.9	5.5	11.1	13.5
	GGSS-3	6.7	8.4	15.6	14.6
	GGSS-CIP	5.2	6.7	NA	NA
Category II	FGSS-1	5.3	6.2	12.5	13.3
	FGSS-2	3.9	5.2	10.3	10.3
	FGSS-CIP	5.2	6.7	NA	NA

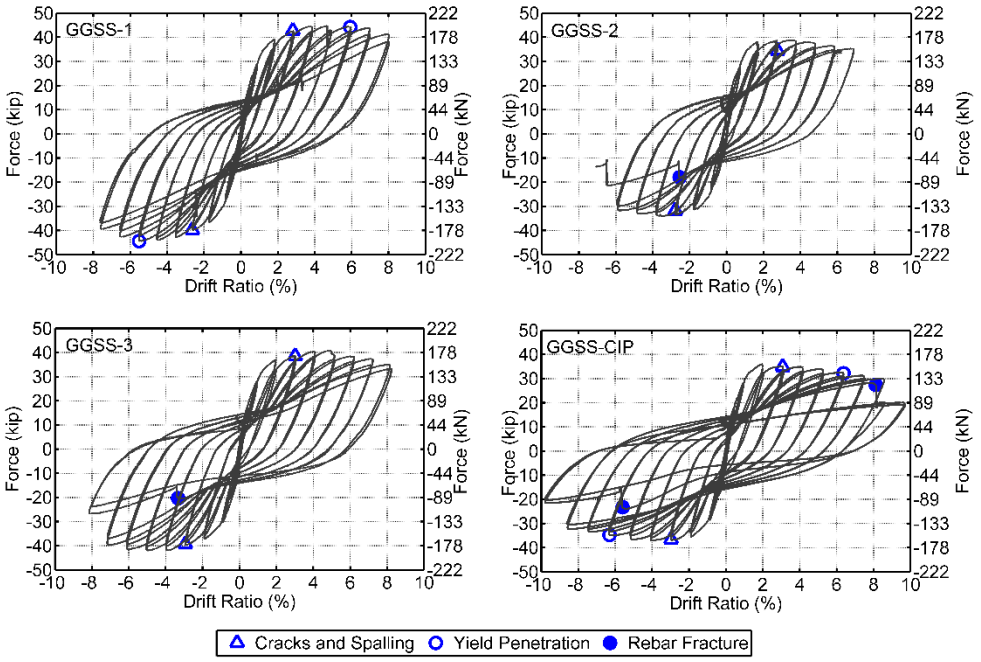

Fig. 6 Hysteresis response of precast and control specimens in Category I

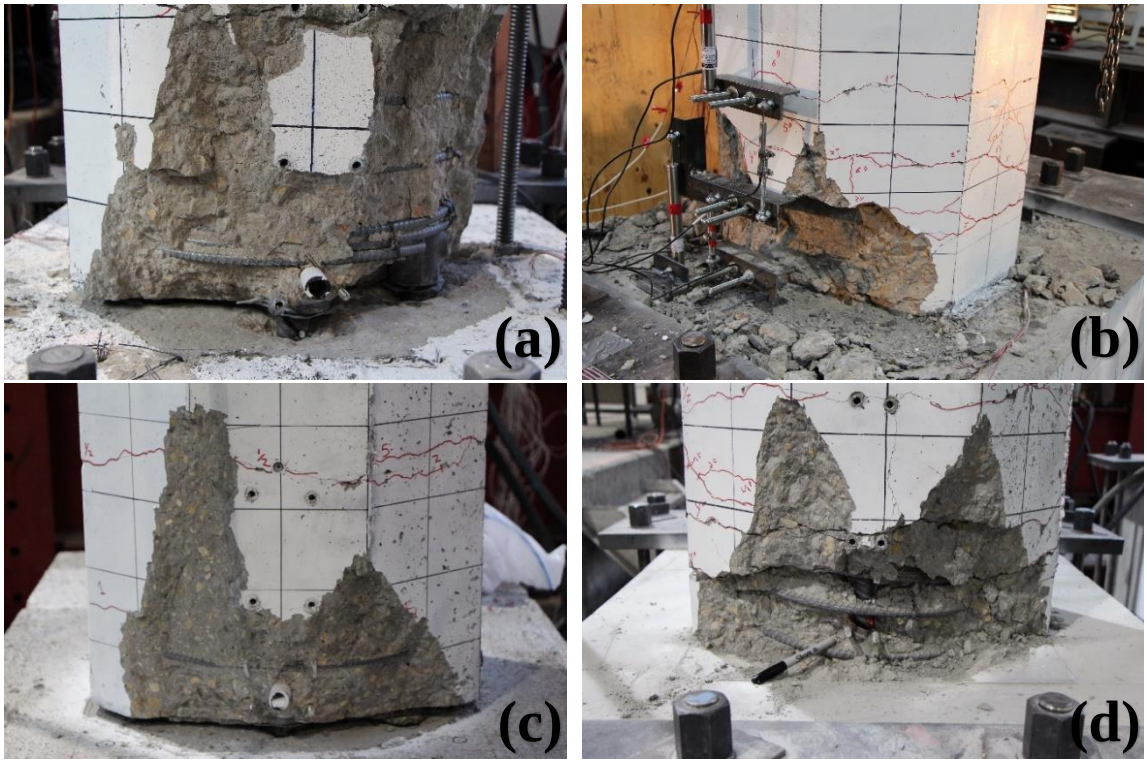

Fig. 7 Damage state at failure for specimens in Category I: (a) GGSS-1, (b) GGSS-2, (c) GGSS-3, (d) GGSS-CIP

Response of GGSS-2

Two hairline flexural cracks developed at sections 12 in. and 28 in. above the column base of GGSS-2 during the 0.5% drift ratio, prior to any crack formation at the interface. The interface gap between the precast column and precast footing became evident during the 1% drift ratio, while a total of nine flexural cracks formed along the column by the end of the 3% drift ratio. The widest crack, located 6 in. above the column base, had a width of 0.03 in. at the end of the 3% drift ratio. Inclined cracks developed on the north and south side of the column base during the 5% drift ratio due to increased tensile demand in the column plastic hinge zone. The extreme east column dowel of GGSS-2 ruptured during the first pull of the 7% drift ratio at a section located 2 in. above the column base. At the end of the experiment, the concrete cover completely spalled at the column base which made the spiral visible over the bottom 8 in. The permanent gap at the column–to–footing interface had a width of 1/16 in. Fig. 7(b) shows the state of damage at the end of the test.

Response of GGSS-3

The damage of GGSS-3 was similar to that of GGSS-1 with the exception of a slightly postponed spalling at the column corners. The crack formation pattern was similar to GGSS-1. The width of the crack that formed above the connectors during the 0.5% drift ratio was 0.013 in. and 0.02 in. after the 5% drift ratio, respectively. The spiral reinforcement became exposed during the 7% drift ratio when the cover concrete crushed completely over the bottom column segment. The gap created at the bed grout section was increased, when the column was at the extreme position, and the footing dowel bars became visible.

During the first pull at the 8% drift ratio, the extreme column reinforcing bar of GGSS-3 fractured at the interface, and the test was terminated as the column strength dropped below 80% of the peak lateral force. Fracture of the bar was attributed to low cycle fatigue as a result of successive bending and re-straightening. A post-test investigation revealed that the cover concrete deteriorated within the lowest 4-in. of the column, and hence, one spiral hoop and the bottom end of the connectors were visible. The bed grout deteriorated in most areas within the interface and loose bed grout pieces were removed from the interface. Damaged concrete was noted around the top portion of the debonded dowel bars in the footing. The crack which had developed earlier at the column–to–footing interface became a 3/32-in. permanent gap at the end of the test. Fig. 7(c) shows the damage at the end of the test.

Response of GGSS-CIP

The overall response of the control specimen was very good as a result of the wide and stable hysteresis loops that implied a relatively high energy dissipation capacity.

Two hairline flexural cracks formed at two sections located 12 in. and 32 in. above the CIP column–to–footing interface, by the end of the 0.5% drift ratio. Spalling initiated at the column corners and a total of nine flexural cracks developed by the end of the 3% drift ratio. The major crack which had developed 4 in. above the column base had a width of 0.06 in. at the end of the 3% drift ratio. Another major crack that had formed 12 in. above the column base earlier became wider and measured 0.007 in. at the end of the 3% drift ratio. During the 5% drift ratio, inclined or flexure-shear type cracks developed on the north and south sides of the column. During the 7% drift ratio, the spalled region grew in such a way that the spiral became partially visible. The extreme west column rebar fractured 1.5 in. above the column base, as a result of low cycle fatigue, slightly before the peak displacement during the second push of the 8% drift ratio, while the extreme east column bar was still undamaged but visible. This reinforcing bar fractured 2 in. above the column base, during the first cycle of the 9% drift ratio, after which the test was terminated. Fig. 7(d) shows the damage state at failure.

EXPERIMENTAL OBSERVATIONS AND HYSTERETIC RESPONSE—CATEGORY II

Fig. 8 shows the hysteresis curves of the column–to–cap beam specimens. They include four major damage states: concrete cracking and spalling, reinforcing bar pullout, yield penetration, and reinforcing bar fracture.

Response of FGSS-1

The pinched hysteresis loops of specimen FGSS-1 indicate that the overall force-displacement performance was controlled by the bond-slip characteristics of the FGSS connectors. In addition to pinching from excessive slippage of the cap beam dowel bars inside the FGSS connectors, reinforcing bar slippage introduced another type of disruption in the unloading branch of the response in the east direction. This was attributed to closure of the gap originally formed as a result of bond deterioration and bar slip. This gap closure phenomenon at the column–to–cap beam interface is visible for the unloading branch of the hysteresis loops at the 4% to 6% drift ratio in the east direction.

All major cracks had developed by the end of the 3% drift ratio. Spalling initiated at the corners of the octagonal column during the first cycle of the 3% drift ratio. The largest crack, which had formed previously at the bed grout section, turned into a gap at the column–to–cap beam interface during the 3% drift ratio.

Cracks widened and concrete spalling progressed at higher drift ratios. During the 6% drift ratio, the cone shape of the expelled grout became visible. The test was terminated after completion of the 6% drift ratio due to bond deterioration, and subsequent reinforcing bar pullout. The height of the spalled concrete was 8 in. and 12 in. on the west and east sides of the column, respectively. The spiral was partially exposed, and the bed grout was crushed at

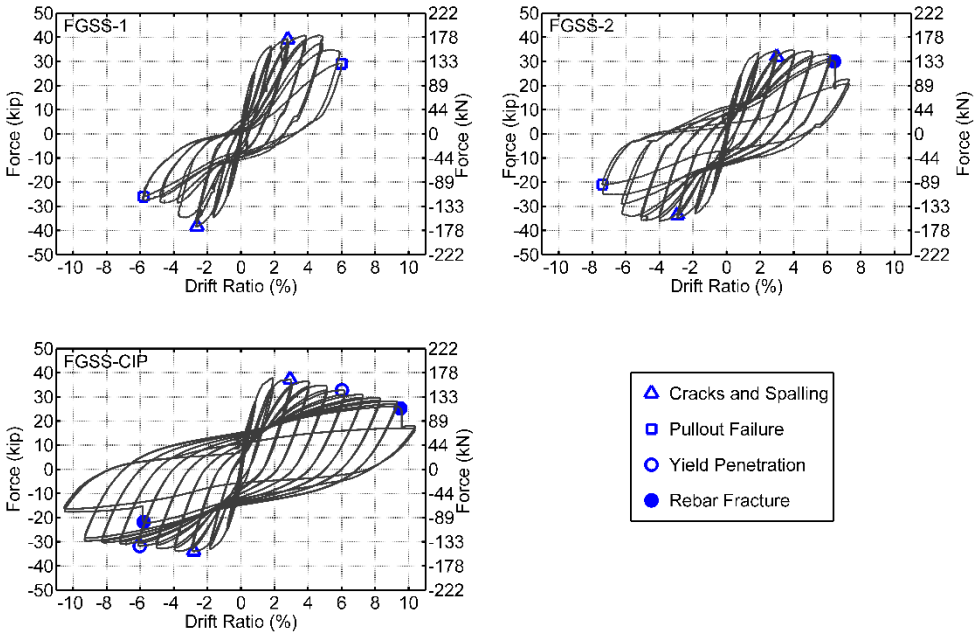

Fig. 8 Hysteresis response of precast and control specimens in Category II

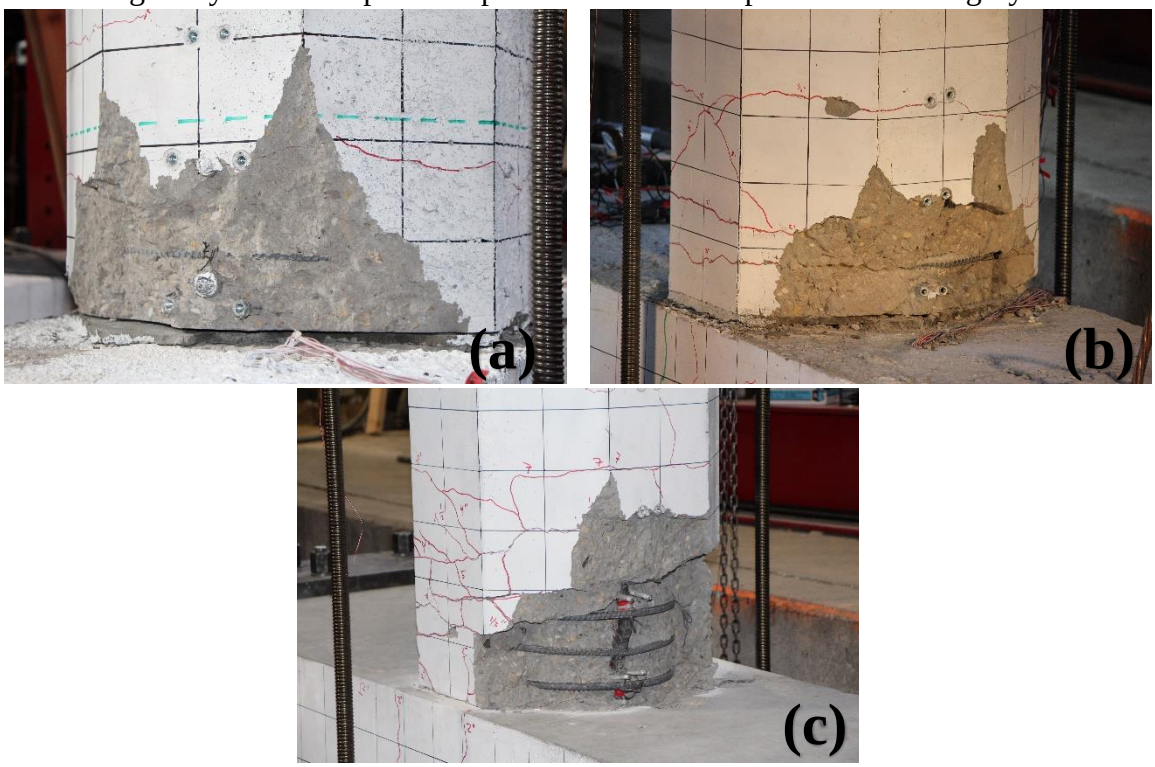

Fig. 9 Damage state at failure for specimens in Category II: (a) FGSS-1, (b) FGSS-2, (c) FGSS-CIP

the column peripheral. The permanent opening at the bed grout had a residual gap equal to 0.1 in. Fig. 9(a) shows the damage in the plastic hinge of the column at failure.

Response of FGSS-2

Hysteresis loops of specimen FGSS-2 were relatively wide and stable compared with specimen FGSS-1, without any considerable strength degradation before reinforcing bar fracture or pullout, in the last drift ratio of 7%. The column west reinforcing bar fractured in the first cycle of the 7% drift ratio, while column east bars underwent excessive slippage, which resulted in strength reduction. Ultimately, the test was terminated after completion of the 7% drift ratio because a strength drop of 42% and 45% as a result of west reinforcing bar fracture and east reinforcing bar pullout. This was a unique failure mode because it included both a ductile failure and a bond-slip failure. The gap closure phenomenon at the column–to–cap beam interface described for FGSS-1 was also observed for this specimen, an indication of excessive reinforcing bar slip at the 4% drift ratio.

A hairline flexural crack formed at a section 12 in. above the column base during the 0.5% drift ratio. During the next drift ratio of 1%, this crack had a width of 0.002 in. Two more flexural cracks developed 20 in. and 28 in. above the column end during the same drift ratio. More cracks developed during the 2% and 3% drift ratio including one at the bed grout. Overall there were seven major flexural cracks that formed along the column by the end of the 3% drift ratio. The crack width formed during the 2% drift ratio at a section 8 in. from the column base, measured 0.03 in. at the end of the 3% drift ratio. Concrete cover spalling initiated during this drift ratio with a height of 8 in. on the column east side. Cracks opened further and concrete spalling intensified after the 3% drift ratio. Flexure-shear cracks formed on the north and south sides of the column during the 5% drift ratio, and the representative crack at 8 in. above the column base had a width of 0.04 in. Spalling became deeper and wider during the 6% drift ratio, and a strength reduction was noted at the end of the second cycle in the west direction. This was attributed to bond deterioration between grout and embedded column dowel. The column extreme west bar broke at the end of the first cycle in the 7% drift ratio, whereas the east bar did not fracture; however, the drop in the lateral force capacity for the west direction implied that a bond-related phenomenon had caused a sudden reduction in strength. Post-test observations showed that the spiral became exposed near the column end, and the largest flexural crack was found 4 in. above the column base measuring 0.06 in. wide. The location of the reinforcing bar fracture was 1 in. above the column base, right below the spiral. Low cycle fatigue was the cause of reinforcing bar fracture as a result of successive bending and straightening of the column extreme bars. A permanent gap equal to 0.125 and 0.0625 in. remained at the bed grout section on the east and west sides of the column, respectively (Fig. 9(b)).

Response of FGSS-CIP

The overall response of specimen FGSS-CIP was satisfactory, and the wide and stable hysteresis loops implied a high energy dissipation capacity. This desirable performance represents a ductile response of a well-detailed reinforced concrete flexural component, under both axial and lateral loading.

A few hairline flexural cracks appeared at the end of the 0.5% drift ratio over a 40 in. long region up from the column end. More hairline flexural cracks developed during the 1% drift ratio, up to 60 in. above the column end. The cracks, which had formed within the lowermost 12 in. portion of the column, grew larger in width during the 2% drift ratio. Also, a 0.03 in. wide crack formed at the column–to–cap beam interface. The crack at 12 in. from the column end had a width of 0.005 in. at this drift ratio. All major flexural cracks developed by the end of the 3% drift ratio, and concrete cover spalling began at the column corners. The crack at the column–to–cap beam interface remained unchanged, while the crack at 12 in. from the column end was 0.01 in. wide.

Inclined cracks formed on the north and south sides of the column base at the 4% drift ratio. By the end of the 4% drift ratio, the largest three cracks measured 0.04 in., 0.06 in., and 0.013 in. wide for the crack at the column–to–cap beam interface, 6 in. from the column end, and 12 in. from the column end, respectively.

Yield penetration was noted around the two column extreme bars at the end of the 6% drift ratio. Spalling became wider and deeper, covering the cracks that developed in the previous cycles. At the 7% drift ratio, the column spiral was visible and the depth of yield penetration increased to 1 1/8 in. The column extreme longitudinal reinforcing bar was visible during the 8% drift ratio. The concrete cover was crushed, which led to buckling of the reinforcing bars during the next drift ratio (Fig. 9(c)).

Low cycle fatigue caused fracture of the column extreme bars on both sides in the first cycle of the 10% drift ratio. The west column bar fractured first when the load was applied in the east direction, and then the east column bar fractured when the load was applied in the west direction. Reinforcing bar fracture occurred in the column end, at 1.0 and 1.5 in. from the cap beam surface for the west and east column bars, respectively. The spalled region had an effective width of 21 in. and height of 8 in., though the maximum height of the spalled area was 16 in. and 20 in. for the east and west column sides, respectively. The cap beam horizontal reinforcing bar was revealed as a result of continuous yield penetration of the column reinforcing bar.

DISPLACEMENT DUCTILITY

Displacement ductility capacity is the ability of a structural component to perform beyond the yield point without excessive strength deterioration; this was computed based on the concept of equal energy of an idealized elasto-plastic system.[19] The average backbone curve was first constructed using the peak values of the first cycle for each drift ratio. To obtain the effective yield displacement of the system, it was assumed that the ideal elasto-plastic curve intersects the average backbone curve at a force equal to 70% times the effective yield force.[15] The ultimate displacement was taken as the displacement corresponding to a 20% drop in lateral load capacity.[20]

Specimens in Category I

The displacement ductility capacity of the GGSS-CIP control specimen was found to be 8.9, compared to displacement ductility values of 5.4, 6.1, and 6.8 achieved by GGSS-1, GGSS-2, and GGSS-3, respectively.

Fig. 10(a) shows the force-displacement response or cyclic envelope, for all specimens in Category I. The force-displacement response revealed a noticeable distinction between precast specimens and GGSS-CIP. The GGSS-CIP control specimen failed by reinforcing bar fracture of the column longitudinal bars, due to low cycle fatigue. Premature rebar fracture was observed for all precast specimens because of higher strain levels concentrated at the end of the GGSS located at the column–to–footing interface.

The overall force-displacement performance of all specimens was similar up to the 1% drift ratio. Specimens GGSS-1 and GGSS-3 had the greatest strength capacity; this was attributed to the rocking mechanism at the column–to–footing interface. Compared to the GGSS-CIP control specimen, the neutral axis of precast specimens was closer to the compression side of the section during the response, causing a higher tension in the reinforcing bars. For the case of GGSS-1 and GGSS-3 with connectors inside the column, the presence of cast-iron sleeve connectors provided the compression required for a larger sectional strength. However, a higher axial load was unintentionally applied to precast specimen GGSS-1 which resulted in a larger lateral force capacity for this specimen. This axial load for GGSS-1 was 60% larger than the axial load applied to GGSS-3. Comparing precast specimen GGSS-3 to cast-in-place specimen GGSS-CIP, it is observed that the lateral force capacity of GGSS-3 was 13% larger than that of GGSS-CIP, on average for both push and pull directions.

Specimens in Category II

Specimen FGSS-CIP had a ductile performance and a displacement ductility of 9.9, which was superior to the precast concrete specimens. The displacement ductility of specimen

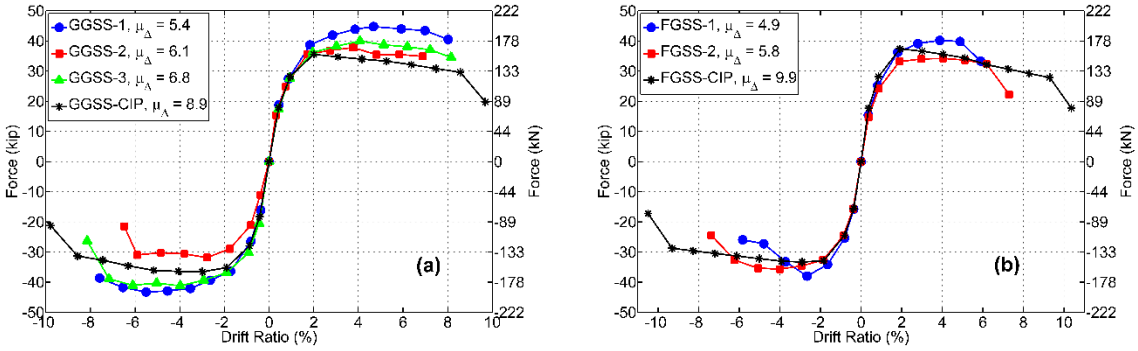

Fig. 10 Force-displacement response: (a) Category I, (b) Category II

FGSS-1 was 4.9, while specimen FGSS-2 had an improved value equal to 5.8 due to a more pronounced bending action along the entire column height.

Fig. 10(b) presents the cyclic envelopes for the three specimens in this category. The response is similar up to 0.5% drift ratio, after which there were differences in the nonlinear response, especially in terms of displacement capacity. The lateral load capacity was similar for specimens FGSS-2 and FGSS-CIP, whereas specimen FGSS-1 had a relatively higher strength. This is attributed to the fact that the axial load applied to specimen FGSS-1 was unintentionally 40% higher than the other two specimens. This is in addition to the rocking mechanism and a larger compressive force component at the interface that was previously discussed for GGSS-1 and GGSS-3. Hence, the lateral force capacity of specimen FGSS-1 was 11% greater than that of specimen FGSS-CIP.

CONCLUSIONS

The experimental evaluation of the column–to–footing and column–to–cap beam joint tests conducted in this research provided qualitative and quantitative measures to evaluate the specimens under quasi-static lateral cyclic loads. More in-depth discussion on the experimental program and results is available in the work of Pantelides et al. (2014) and Ameli et al. (2015).[21, 22] A summary of findings is offered:

- Control specimens GGSS-CIP and FGSS-CIP had a good hysteretic response with ductile failure (reinforcing bar fracture on opposite sides of the column). Well-distributed flexural cracks formed along the column height and the concrete cover spalled completely at the column end. The overall performance of the control specimens was dominated by flexural action and formation of a plastic hinge at the column end. More localized damage was observed for precast concrete specimens GGSS-1, GGSS-3, and FGSS-1 with the connectors in the column. This involved fewer flexural cracks along the column height compared to the control specimens.

The spalled region was also smaller as a result of the presence of the grouted splice sleeve connectors in the column. Precast concrete specimens GGSS-2 and FGSS-2 with the grouted splice sleeve connectors in the footing or cap beam, respectively, had a damage state similar to the control specimens because there were no sleeve connectors in the column.

For the precast column–to–footing specimens with grouted/grouted splice sleeve connectors:

- Reinforcing bar fracture occurred for all precast alternatives and the control specimen which indicated that the bond between reinforcing bars and high-strength grout was good. Hence, a ductile performance was achieved for all specimens until bar fracture. The fracture of reinforcing bars in all specimens was because of low cycle fatigue.
- Precast specimen GGSS-1 (connectors in the column) had a displacement ductility of 5.4. A more ductile response with a better hysteretic performance was achieved for precast specimen GGSS-2 with connectors inside the footing. The eight bar diameter debonded rebar zone for the footing dowel bars which was implemented for specimen GGSS-3 (connectors in the column) resulted in a displacement ductility of 6.8. The cast-in-place control specimen had a displacement ductility of 8.9 with hysteresis loops that were wide and stable, implying excellent energy dissipation and hysteretic performance. The displacement ductility obtained for all test alternatives exceeded the minimum component displacement ductility of 3.0 specified in the Caltrans SDC. In addition, the displacement ductility values were greater than the maximum displacement ductility of 5 which was specified in the AASHTO Seismic Guide for single-column bridge bents.
- Precast specimen GGSS-3, constructed with grouted/grouted splice sleeve connectors in the column and debonded reinforcing bars in the footing, achieved a drift capacity of 8.0%, which exceeds the drift demand expected in large earthquakes; thus, it achieved satisfactory hysteretic performance and energy dissipation. Precast concrete joints constructed with the specific details of specimen GGSS-3 are expected to perform adequately in moderate to high seismic regions, i.e. SDC C and D per AASHTO Seismic Guide.

For the precast column–to–cap beam specimens with fastened/grouted splice sleeve connectors:

- Reinforcing bar fracture for specimen FGSS-CIP occurred at a 10% drift ratio due to low cycle fatigue. Premature reinforcing bar fracture occurred in the west column bar of specimen FGSS-2 at a 7% drift ratio, which was accompanied by pullout failure of the east column bar. Specimen FGSS-1 failed early at a drift ratio of 6% because of reinforcing bar pullout due to excessive bond slip.

- Specimen FGSS-CIP had a displacement ductility of 9.9 with hysteresis loops that were wide and stable, implying excellent energy dissipation. A displacement ductility of 5.8 was achieved for specimen FGSS-2 for which the fastened/grouted splice sleeve connectors were inside the cap beam. Compared with specimen FGSS-1, with a displacement ductility of 4.9, a more ductile response along with a better hysteretic performance was obtained by placing the fastened and grouted splice sleeve connectors in the cap beam. The displacement ductility obtained for all alternatives exceeded the minimum component displacement ductility of 3.0 specified in the Caltrans SDC. The displacement ductility for specimen FGSS-2 was greater than the maximum ductility of 5.0 for single-column bridge bents but less than the maximum ductility of 6.0 for multiple-column bridge bents specified in the AASHTO seismic guide for ductile members in high seismic zones.
- Precast specimen FGSS-2, constructed with fastened/grouted splice sleeve connectors in the cap beam, achieved a drift capacity of 7.0%, which exceeds the drift demand expected in large earthquakes; thus, it achieved satisfactory hysteretic performance and energy dissipation. In addition it achieved a displacement ductility of 5.8 and a curvature distribution that closely emulates cast-in-place construction. Precast concrete joints constructed with the specific details of specimen FGSS-2 are expected to perform adequately in moderate to high seismic regions, i.e. SDC C and D per AASHTO Seismic Guide.

ACKNOWLEDGEMENTS

The authors would like to acknowledge the financial support of the Utah, New York State, and Texas Departments of Transportation, and the Mountain-Plains Consortium. The authors wish to thank Dr. Lawrence D. Reaveley, Professor Emeritus at the University of Utah, for his invaluable input throughout the project. Special thanks are extended to Mark Bryant of the University of Utah for his untiring efforts and support. The authors greatly appreciate the valuable input offered by Carmen Swanwick and Joshua Sletten of UDOT, and Harry White of NYSDOT. The authors are also grateful for the donation of materials by Splice Sleeve North America and ERICO, and the assistance of Hanson Structural Precast.

REFERENCES

1. Marsh, M. L., Wernly, M., Garett, B. E., Stanton, J. F., Eberhard, M. O., and Weinert M. D., “Application of Accelerated Bridge Construction Connections in Moderate-to-High Seismic Regions,” *NCHRP Report 698*, National Cooperative Highway Research Program, Washington, DC, 2011.
2. ACI Committee 439, “Types of Mechanical Splices for Reinforcing Bars,” American Concrete Institute, Farmington Hills, MI, 2007.

3. Jansson, P. O., "Evaluation of Grout-Filled Mechanical Splices for Precast Concrete Construction," *Report R-1512*, Michigan Department of Transportation, Lansing, MI, 2008.
4. Rowell, S. P., Grey, C. E., Woodson, S. C., and Hager, K. P., "High Strain Rate Testing of Mechanical Couplers," Report ERDC TR-09-8, Washington, DC, 2009.
5. Haber, Z. B., M. S. Saiidi, and D.H. Sanders. 2013. "Precast Column-Footing Connections for Accelerated Bridge Construction in Seismic Zones." *CCEER 13-08*. Reno, NV: Center for Civil Engineering Earthquake Research, Department of Civil and Environmental Engineering, University of Nevada, Reno.
6. Splice Sleeve Japan, Ltd, "Tests on Re-Bar Splices in Reinforced Concrete Columns Using NMB Splice Sleeves," *Report NPD-024*, Splice Sleeve Japan, Ltd., Tokyo, Japan.
7. Matsuzaki, Y., "Effects of Sleeves on Member Properties, Study on the Behavior of Reinforced Concrete Beams with Grout-Filled Steel Splice Sleeves," Architectural Institute of Japan, 1987.
8. Reetz, R. J., Ramin, M. V., and Matamoros, A., "Performance of Mechanical Splices within the Plastic Hinge Region of Beams Subject to Cyclic Loading," *Proceedings of 13th World Conference on Earthquake Engineering*, Vancouver, B.C., Canada, 2004.
9. Aida, H., Tanimura, y., Tadokoro, T., and Takimoto, K., "Cyclic Loading Experiment of Precast Columns of Railway Rigid-Frame Viaduct Installed with NMB Splice Sleeves," *Proceedings of the Japan Concrete Institute*, V. 27, No. 2, 2005.
10. Tazarv, M., and Saiidi, M. S., "Next Generation of Bridge Columns for Accelerated Bridge Construction in High Seismic Zones." *CCEER 14-06*, Center for Civil Engineering Earthquake Research, Department of Civil and Environmental Engineering, University of Nevada, Reno, Reno, NV, 2014.
11. Haber, Z. B., Saiidi, M. S., and Sanders. D. H., "Seismic Performance of Precast Columns with Mechanically Spliced Column-Footing Connections," *ACI Structural Journal*, V. 111, No. 3, 2014, pp. 639-650.
12. American Association of State Highway and Transportation Officials (AASHTO). "AASHTO LRFD Bridge Design Specifications," Washington, DC, 2012.
13. American Association of State Highway and Transportation Officials (AASHTO). "AASHTO Guide Specifications for LRFD Seismic Bridge Design," Washington, DC, 2011.
14. California Department of Transportation, "Seismic Design Criteria," Division of Engineering Services, Sacramento, CA, 2010.
15. ACI Committee 374, "Guide for Testing Reinforced Concrete Structural Elements Under Slowly Applied Simulated Seismic Loads," American Concrete Institute, Farmington Hills, MI, 2013.
16. ASTM A370-09a. 2009. Standard Test Method and Definitions for Mechanical Testing of Steel Products. West Conshohocken, PA: ASTM International. doi: 10.1520/A0370-09A.
17. ASTM C39. 2012. Standard Test Method for Compressive Strength of Cylindrical Concrete Specimens. ASTM International, West Conshohocken, PA. doi: 10.1520/C0039_C0039M-12.

18. ASTM C109. 2012. Standard Test Method for Compressive Strength of Hydraulic Cement Mortars (Using 2-in. or [50-mm] Cube Specimens). ASTM International: West Conshohocken, PA. doi: 10.1520/C0109_C0109M-12.
19. Park, R., "Evaluation of Ductility of Structures and Structural Assemblages from Laboratory Testing," *Bulletin of the New Zealand National Society for Earthquake Engineering*, V. 22, No. 3, 1989, pp. 155–166.
20. Priestley, M. J. N., and Park, R., "Strength and Ductility of Concrete Bridge Columns under Seismic Loading," *ACI Structural Journal*, V. 84, No. 1, 1987, pp. 61–76.
21. Pantelides, C.P.; Ameli, M. J.; Parks, J.E.; and Brown, D.N., 2014. "Seismic Evaluation of Grouted Splice Sleeve Connections for Precast RC Bridge Piers in ABC." Utah Department of Transportation Research Division; *Report No. UT-14.09*.
22. Ameli, M. J., Parks, J. E., Brown D. N., and Pantelides, C. P., "Seismic Evaluation of Grouted Splice Sleeve Connections for Reinforced Precast Concrete Column-to-Cap beam Joints in Accelerated Bridge Construction," *PCI Journal*, V. 60, No. 2, 2015, pp. 80-103.